

Article

Hydrogenation production from ammonia borane over PtNi alloy nanoparticles immobilized on graphite carbon nitride

Mingya Zhang ¹, Xue Xiao ^{1,2}, Yan Wu ², Yue An ⁴, Lixin Xu ^{2,3} and Chao Wan ^{2,3,4*}

¹ Key Laboratory of Metallurgical Emission Reduction & Resources Recycling, Ministry of Education, School of Metallurgical Engineering, Anhui University of Technology, Ma'anshan 243002, China; 525071395@qq.com (M.Z.)

² School of Chemistry and Chemical Engineering, Anhui Province Key Laboratory of Coal Clean Conversion and High Valued Utilization, Anhui University of Technology, Ma'anshan 243002, China; 1219738904@qq.com(X.X.); 1115945327@qq.com(Y.W.); lxx@hotmail.com(L.X.)

³ Ahut Chemical Science & Technology Co., Ltd, Ma'anshan 243002, China;

⁴ College of Chemical and Biological Engineering, Zhejiang University, Hangzhou 310027, China; zju.anyue@hotmail.com

* Correspondence: wanchao1219@hotmail.com(C.W.); Tel: +86 555 2311807(C.W.); Fax: +86 555 2311822(C.W.);

Abstract: Graphite carbon nitride (g-C₃N₄) supported PtNi alloy nanoparticles (NPs) were fabricated *via* a facile and simple impregnation and chemical reduction method and explored their catalytic performance towards hydrogen evolution from ammonia borane (AB). Interestingly, the resultant Pt_{0.5}Ni_{0.5}/g-C₃N₄ catalyst affords superior performance, including 100% conversion, 100% H₂ selectivity, yielding the extraordinary initial total turnover frequency (TOF) of 250.8 mol_{H₂} min⁻¹ (mol_{Pt})⁻¹ for hydrogen evolution from AB at 10 °C, a relatively low activation energy of 38.09 kJ mol⁻¹, and a remarkable reusability (at least 10 times), which surpass most of the noble metal heterogeneous catalysts. This notably improved activity is attributed to the charge interaction between PtNi NPs and g-C₃N₄ support. Especially, the nitrogen-containing functional groups on g-C₃N₄, serving as the anchoring sites for PtNi NPs, may be beneficial for becoming a uniform distribution and decreasing the particle size for the NPs. Our work not only provides a cost-effective route for constructing high-performance catalysts towards the hydrogen evolution of AB but also prompts the utilization of g-C₃N₄ in energy fields.

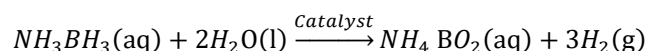
Keywords: Ammonia borane; PtNi/g-C₃N₄; Hydrogen storage; Dehydrogenation

1. Introduction

With the ever-growing consumption of fossil energy, accompanying with seriously environmental issues, searching for green, sustainable, abundant and alternative energy sources is of burgeoning urgency [1,2]. Hydrogen, as a clean energy source, has attracted significant research interest owing to its distinctive merits such as producing only water as a by-product and possessing more energy density than that of fossil fuels [3-5]. However, hydrogen, possessing the feature of low density, makes it difficult to liquefy and compress, thus hindering the large-scale applications [4-6]. Therefore, the exploration and seek for hydrogen storage materials with outstanding performance remains a challenging issue.

Tremendous efforts, in the past decades, have been made to explore and design hydrogen storage materials such as hydrazine, formic acid, and ammonia borane and so forth[7-13]. Among various hydrogen storage materials conducted, ammonia borane (AB), a white solid with excellent stability at room temperature and high hydrogen content (19.6 wt %), has aroused considerable interest as a promising hydrogen storage material [14,15]. There are two main approaches for AB to release hydrogen: (i) thermal dehydrogenation, (ii) hydrolysis dehydrogenation[14-16]. However,

compared with thermal dehydrogenation, proceeding under high temperature, hydrolysis dehydrogenation process is easier to accomplish the industrial application under mild conditions [15–17]. With the aid of the suitable catalyst, 1 mol of AB can be controlled to release 3 mol of hydrogen under moderate conditions. The catalytic hydrolysis reaction can be described in detail as follows [18–22]:



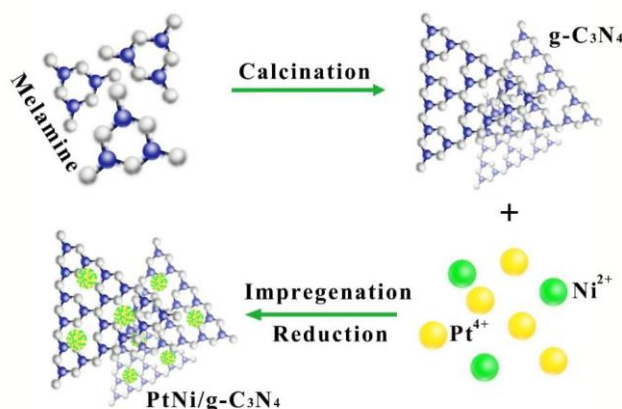
In recent years, a large number of supported metal catalysts including noble metal and non-noble metal, have been constructed for the hydrolysis of AB, among which Pt-based catalysts, as one of the most studied catalysts both in industrial and scientific fields, demonstrate more extraordinary catalytic performance than that of other metal catalysts for hydrolysis of AB [20–27]. However, the features of Pt with its high prices and limited reserves severely restrict its extensive utilization of Pt metal as the catalyst [27–29]. Currently, to actually reduce the utilization amount of Pt, assembling with the enhancement of catalysts, the fabrication of Pt alloy nanomaterials, especially coupling with the noble-free metals, such as Fe, Co, and Ni *etc.*, has been identified to be an effective approach due to its structural and electronic effects [30–33]. Previous studies have revealed that Pt-M bimetallic catalysts could display higher catalytic activity than that of their single counterparts as well as lower cost [32–36]. For instance, Han *et al.* applied a chemical reduction route to synthesize amino modified SiO₂ nanospheres supported CoPt-Co hybrid at 278 K, affording a turnover frequency (TOF) value of 25.59 mol_{H₂}min^{−1}mol_M^{−1}, almost two-fold as high as that of unsupported Pt_{0.1}Co_{0.9} NPs [37]. Xu *et al.* fabricated hierarchical nanoporous PtCu alloy nanoflowers by means of the two-step dealloying method with a maximum TOF value up to 108 mol_{H₂}min^{−1}mol_M^{−1} [38]. Lu *et al.* reported the synthesis of PtNi/NiO Clusters Coated by Hollow Silica using atomic sacrifice method, reaching a TOF of 1240.3 mol_{H₂}min^{−1}mol_{Pt}^{−1} [39]. However, Pt-M NPs are readily tending to aggregate to form a bigger particle, resulting in a momentous decrease in the catalytic performance including activity, stability, and efficiency. Therefore, in order to obtain high catalytic performance for hydrolytic dehydrogenation of AB, considerable effort have been devoted to fabricate high efficiency catalysts involving many types of supporting materials.

It is noted that assembling alloy with appropriate supports, such as metal oxides, carbon nanotubes, mesoporous carbon nitride and graphene *etc.*, emerges as one of novel encouraging approach to further improve the catalytic activities and stability [39–46]. It is well known that the supporting materials play a critical role in enhancing its catalytic properties due to the synergistic effects between alloy and supports. Graphitic carbon nitride (g-C₃N₄), a promising two-dimensional non-metal material, is regarded as a promising candidate owing to its attractive electronic structure, high nitrogen content, excellent chemical and thermal stability, and environment friendliness [45–48]. Chen *et al.* constructed Au-Co nanoparticles (Au-Co@CN), displaying exceedingly good catalytic activity with a TOF value reaching 2897 mol H₂mol_{metal}^{−1}h^{−1} at 298 K [49]. Fan *et al.* reported the *in-situ* construction of g-C₃N₄ supported Rh NPs, giving a very high TOF value of 969 mol H₂mol_{Rh}^{−1}h^{−1} [50]. Encouraged by these achievements, the construction of PtNi alloy anchored into g-C₃N₄ for hydrogen production from the hydrolysis of AB is of paramount significance and has rarely been reported. Additionally, investigating the construction of bi-metal NPs in g-C₃N₄ as well as the exploration of the synergistic effect between them are also of outmost importance.

Hence, in this work, we focused on the construction of PtNi with different ratios immobilized on g-C₃N₄, preparing *via* the direct pyrolysis of melamine under nitrogen atmosphere [51,52], through a simple impregnation and co-reduction method under an ambient atmosphere. The resulting materials were evaluated as catalysts towards the hydrogen production from AB under mild conditions. The influence of some parameters, such as metal concentration, catalyst concentration, AB concentration, and reaction temperature, on the catalytic performance of PtNi/g-C₃N₄ were conducted in detail. Especially, the Pt_{0.5}Ni_{0.5}/g-C₃N₄ demonstrates optimal catalytic performance for the hydrolysis of AB compared with the samples of other molar ratio of PtNi. Furthermore, the stability of the optimum catalyst was investigated as well.

2. Results and Discussion

The synthesis process of PtNi/g-C₃N₄ is schematically emerged in Scheme 1. Typically, g-C₃N₄ was prepared *via* a direct pyrolysis route employing melamine as precursor. Then, the Pt and Ni precursor with different contents immobilized on g-C₃N₄ was fabricated, using a simple impregnation and reduction process, where sodium borohydride is employed as a reducing agent, and then applied as catalysts towards hydrogen production of AB. The accurate composition of PtNi/g-C₃N₄ was analyzed by inductively coupled plasma atomic emission spectroscopy (ICP-AES), which are close to their desired contents (Table S1). As displayed in Table S1, the BET specific areas of PtNi/g-C₃N₄ is around 10 m²/g, which is close to the values reported in the literature [51,52]. Figure. 1 shows the XRD patterns of PtNi/g-C₃N₄ with different contents.



Scheme 1. Schematic illustration of the fabrication of PtNi/g-C₃N₄.

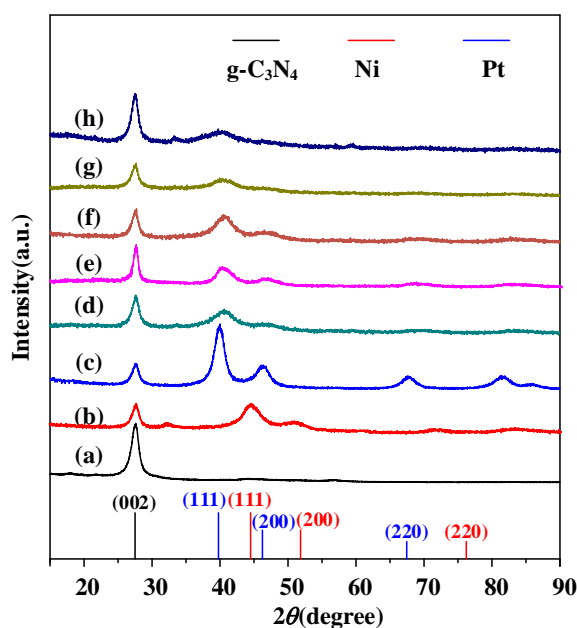


Figure 1. XRD patterns of PtNi/g-C₃N₄ composites with different molar ratio of PtNi: (a) g-C₃N₄, (b) Ni/g-C₃N₄, (c) Pt/g-C₃N₄, (d) Pt_{0.8}Ni_{0.2}/g-C₃N₄, (e) Pt_{0.6}Ni_{0.4}/g-C₃N₄, (f) Pt_{0.5}Ni_{0.5}/g-C₃N₄, (g) Pt_{0.4}Ni_{0.6}/g-C₃N₄, (h) Pt_{0.2}Ni_{0.8}/g-C₃N₄.

It is evident that a strong peak at 27.5° for all samples is attributed to the (200) plane of g-C₃N₄. For Ni/g-C₃N₄, other than the characteristic peak of g-C₃N₄, there are three peaks centered at 44.5°, 51.8°, 76.4°, respectively, which can be ascribed to the (111), (200) and (220) planes of Ni (JCPDS no: 65-0380). For Pt/g-C₃N₄, three peaks at 39.8°, 46.2° and 67.5° are assigned to the (111), (200) and (220) planes of Pt (JCPDS no: 65-2868). Furthermore, it is evident that a shift to higher angle compared to that of the Pt (111) peak in Pt/g-C₃N₄, indicating that PtNi is existed in the form of alloy, which is consistent with the previous literatures yet reported [39,53-55]. The chemical structures of g-C₃N₄, Pt/g-C₃N₄, Ni/g-C₃N₄ and Pt_{0.5}Ni_{0.5}/g-C₃N₄ were further investigated by Fourier transform infrared

(FTIR), as presented in Figure 2. A similar FT-IR spectra can be observed for all samples. An obvious absorption peak centered at 810 cm^{-1} for all samples is ascribed to the bending vibration of the s-triazine ring. A series of peaks detected in $1200\text{--}1600\text{ cm}^{-1}$ are identified as the stretching modes of aromatic CN heterocycles. In addition, the broad absorption ranging from $3000\text{ to }3400\text{ cm}^{-1}$ is attributed to the stretching mode of O-H (adsorbed water molecules) and N-H (amino groups) [31–36,51,52].

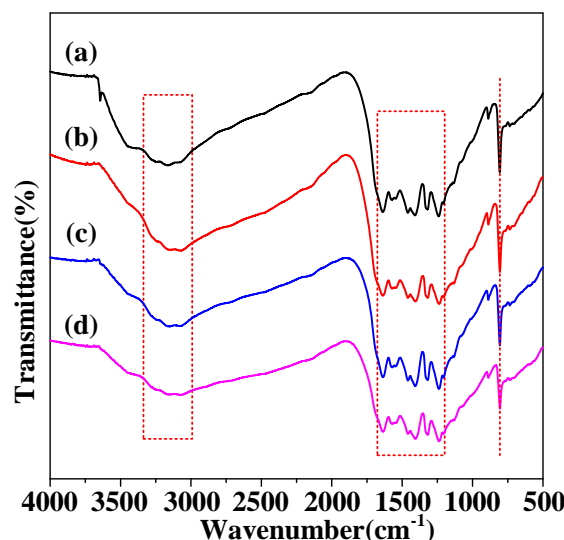


Figure 2. FT-IR spectra of (a) g-C₃N₄, (b) Pt/g-C₃N₄, (c) Ni/g-C₃N₄ and (d) Pt_{0.5}Ni_{0.5}/g-C₃N₄.

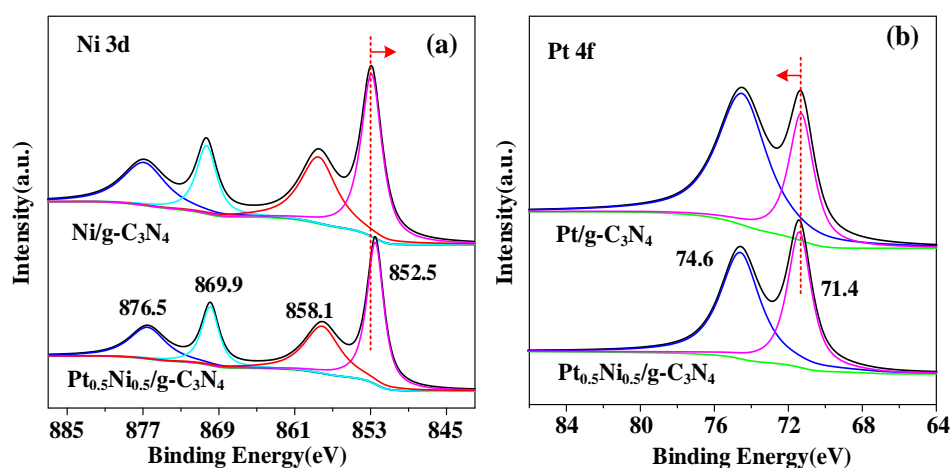


Figure 3. XPS spectra for catalyst Ni/g-C₃N₄, Pt/g-C₃N₄ and Pt_{0.5}Ni_{0.5}/g-C₃N₄ showing (a) Ni 2p, and (b) Pt 4f.

To gain the valence state of Pt and Ni, XPS analysis is employed for Pt_{0.5}Ni_{0.5}/g-C₃N₄, and the result is illustrated in Figure 3, which presents the characteristic peaks for Pt and Ni, thus implying the coexistence of both metals. The binding energy (BE) of C and N in Pt_{0.5}Ni_{0.5}/g-C₃N₄ are in accordance with the previous reported literatures about g-C₃N₄ (Figure S1) [50–52]. As given in Figure 3(a), the BE observed at 852.5 and 869.9 eV are ascribed to the Ni 2p_{3/2} and Ni 2p_{1/2} of metallic Ni, respectively. The oxidized Ni centered at 858.1 and 876.5 eV are detected, which may likely attribute to the sample treatment route for the XPS measurements, as revealed before [56–58]. The BE of 71.4 and 74.6 eV in Figure 3(b) are corresponded to the Pt 4f_{7/2} and Pt 4f_{5/2} of metallic Pt. In addition, there is a positive shift toward 0.1 eV for the BE of Pt in Pt_{0.5}Ni_{0.5}/g-C₃N₄ compared with that of pure Pt, while a negative shift with 0.4 eV could be observed for Ni in Pt_{0.5}Ni_{0.5}/g-C₃N₄ in comparison with that of pure Ni, thereby confirming the formation of PtNi alloy, which is good agreement with those of alloy previously reported [56–61].

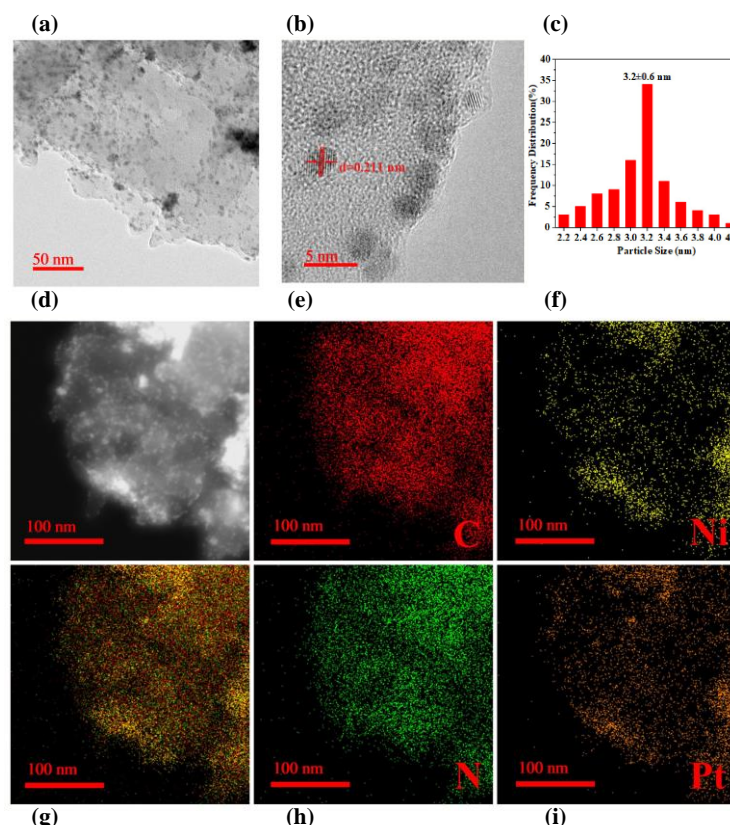


Figure 4. (a) TEM images of $\text{Pt}_{0.5}\text{Ni}_{0.5}/\text{g-C}_3\text{N}_4$, (b) amplified HRTEM image of $\text{Pt}_{0.5}\text{Ni}_{0.5}/\text{g-C}_3\text{N}_4$, (c) Particle size distribution of $\text{Pt}_{0.5}\text{Ni}_{0.5}$ NPs, (d) HAADF-STEM image and (e-i) elemental mapping images of $\text{Pt}_{0.5}\text{Ni}_{0.5}/\text{g-C}_3\text{N}_4$.

To further explore the morphology and microstructure of the $\text{Pt}_{0.5}\text{Ni}_{0.5}/\text{g-C}_3\text{N}_4$ catalyst, we conducted TEM, high-angle annular dark-field scanning transmission electron microscopy (HAADF-STEM) and EDS measurements, as depicted in Figure 4 (a-i). The TEM images of $\text{Ni/g-C}_3\text{N}_4$ reveal that almost all the nanoparticles are uniformly dispersed into the surface of $\text{g-C}_3\text{N}_4$ with an average size of ~ 4.3 nm (Figure S2(a,b)). Furthermore, for $\text{Pt/g-C}_3\text{N}_4$, there are many homogeneous distribution of nanoparticles with their size ranging from 3.6 to 6.0 nm, as depicted in Figure S2 (d,e). However, TEM images reveal that the PtNi nanoparticles in $\text{Pt}_{0.5}\text{Ni}_{0.5}/\text{g-C}_3\text{N}_4$ catalyst have a uniform diameter distribution with a mean diameter of ~ 3.2 nm and are homogeneously dispersed on the surface of $\text{g-C}_3\text{N}_4$ (Figure 4 (a-c)), which may be due to the alloy effect. Figure 4 (b) presents that the d-spacing of the particle is 0.211 nm, which differs from the (111) plane of Pt (0.227 nm) (Figure S2(f)) and Ni (0.204 nm) (Figure S2(c)), further revealing that $\text{Pt}_{0.5}\text{Ni}_{0.5}$ is in the form of alloy state [54–56, 58–61]. The energy dispersive X-ray (EDX) result (Figure S3) further verifies the coexistence of Pt and Ni in the $\text{Pt}_{0.5}\text{Ni}_{0.5}/\text{g-C}_3\text{N}_4$. A representative high-angle annular dark-field scanning TEM (HAADF-STEM) image confirmed the homogeneous distribution of Pt and Ni elements on the $\text{g-C}_3\text{N}_4$ catalyst surface at the same position (Figure 4 (d-i)), which confirms again the formation of a PtNi alloy.

Figure 5(a) presents the hydrogen release from AB catalyzed by $\text{Pt}_x\text{Ni}_{1-x}/\text{g-C}_3\text{N}_4$ catalyst with different components. Among all the $\text{Pt}_x\text{Ni}_{1-x}/\text{g-C}_3\text{N}_4$ conducted, $\text{Pt}_{0.5}\text{Ni}_{0.5}/\text{g-C}_3\text{N}_4$ reveals optimum catalytic performance towards the dehydrogenation of AB in comparison with that of other molar ratio of $\text{Pt}_x\text{Ni}_{1-x}/\text{g-C}_3\text{N}_4$. The hydrogen production from AB over $\text{Pt}_{0.5}\text{Ni}_{0.5}/\text{g-C}_3\text{N}_4$ can be completed within only 1.5 min, giving a TOF value of $250.8 \text{ mol}_{\text{H}_2} \text{ min}^{-1} (\text{mol}_{\text{Pt}})^{-1}$ (Figure 5(b)), which is the highest as compared with other as-prepared PtNi alloy catalysts, as well higher than most reported Pt-based or other noble metal-based catalysts towards the hydrogen evolution of AB as displayed in Table 1 [38,40,62–68]. The results showed that the platinum coupling with nickel could significantly improve the hydrolytic activity of AB. The superior catalytic performance of the $\text{Pt}_{0.5}\text{Ni}_{0.5}/\text{g-C}_3\text{N}_4$ can be

ascribed to the synergetic effect between Pt and Ni atoms as well as the enhanced interaction between PtNi NPs and g-C₃N₄.

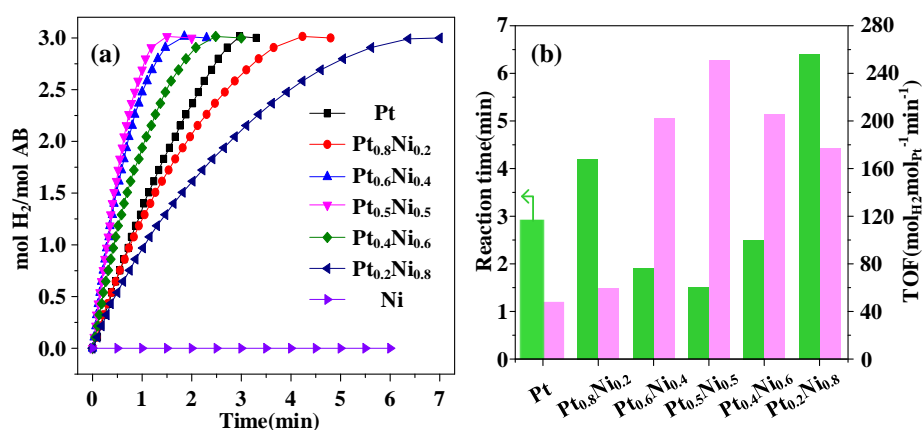


Figure 5. (a) Time plots of catalytic dehydrogenation of AB (4 mmol) by PtNi/g-C₃N₄ catalyst with different ratios at 10 °C; (b) Time needed to complete the reaction and TOF values (obtained based on the overall Pt moles) of the PtNi/g-C₃N₄ catalysts.

Table 1. Catalytic activities and the activation energy of catalysts in the hydrolysis of AB.

Catalysts	TOF(mol _{H2} min ⁻¹ mol ⁻¹ _M)M=Pt, Ru, Ag	E _a (kJ mol ⁻¹)	Refs.
Pt _{0.5} Ni _{0.5} /g-C ₃ N ₄	250.8	38.09	This work
NP-Pt ₄₀ Co ₆₀ composite	131	38.8	40
Pt@SiO ₂	158	53.6	62
PtRu	59.6	38.9	63
RuCu/graphene	135	30.89	64
Pt/CeO ₂ /RGO	48	-	65
RuCo(1:1)/γ-Al ₂ O ₃	32.9	47	66
Pt _{0.65} Ni _{0.35}	44.3	39.0	67
hnp-Pt ₃₅ Cu ₆₅	108	40.5	38
Pd-Pt@PVP NPs	125	51.7	68

Given that Pt_{0.5}Ni_{0.5}/g-C₃N₄ demonstrates the best catalytic performance towards the dehydrogenation of AB in this work, Pt_{0.5}Ni_{0.5}/g-C₃N₄, as the representative, is selected to further explore its dehydrogenation kinetics. As illustrated in Figure 6(a), the catalyst concentrations-dependent test of Pt_{0.5}Ni_{0.5} NPs was investigated at 10 °C by modifying the catalyst concentration ranging from 6.25 to 25 mM. The hydrogen generation rate demonstrate an obvious upward tendency with the increasing of catalyst concentrations. The relation between logarithmic plots of dehydrogenation rate and catalyst concentrations is illustrated in Figure 6(b). The slope of straight line was estimated to be 1.08, implying that the dehydrogenation reaction is first-order in term of the catalyst concentration. Furthermore, to explore the influence of AB concentration on the dehydrogenation of AB, a series of experiments with different concentrations of AB were performed, where the AB concentrations were modulated from 250 to 1000 mM, as shown in Figure 6(a), and Pt_{0.5}Ni_{0.5}/g-C₃N₄ NPs was kept at 0.100g. Figure 7(a) shows corresponding hydrogen amount versus time. As the concentration of AB increased, the dehydrogenation reaction time increased clearly from 0.8 to 1.5 min. Figure 7(b) displays logarithmic plots of dehydrogenation rate versus AB

concentrations, where the line slope is 0.05, suggesting that the dehydrogenation reaction of AB presents zero-order regarding the catalyst concentrations.

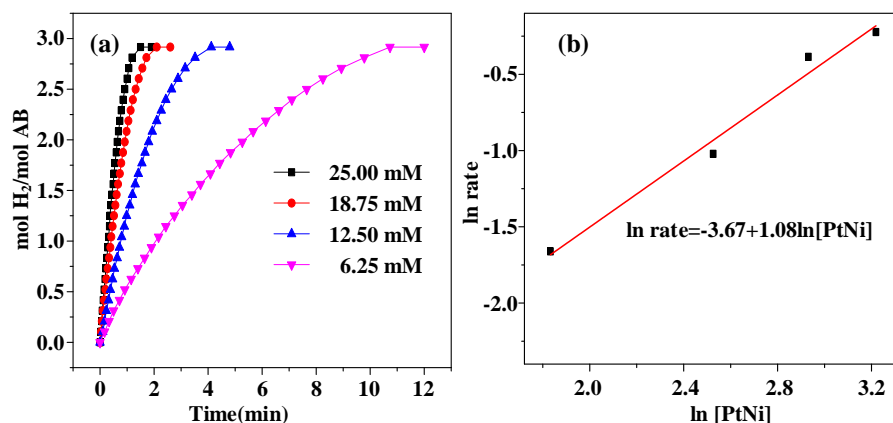


Figure 6. (a) Plots of moles of H₂ per mole of AB versus time for the hydrolysis of AB (4 mmol) in the presence of Pt_{0.5}Ni_{0.5}/g-C₃N₄ (0.1 g) at different catalyst concentrations at 10 °C, (b) The logarithmic plot of hydrogen evolution rate versus PtNi concentrations.

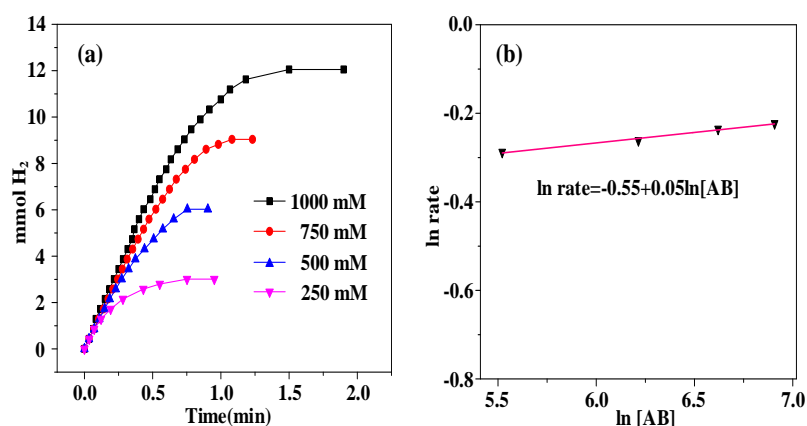


Figure 7. (a) Plot of H₂ volume versus time for hydrogen generation from AB hydrolysis catalyzed by Pt_{0.5}Ni_{0.5}/g-C₃N₄ catalyst at different AB concentrations ([Pt_{0.5}Ni_{0.5}/g-C₃N₄]=0.100 g, T=10 °C), (b) The logarithmic plot of hydrogen evolution rate versus AB concentrations.

To explore the influence of temperature, the AB concentration was maintained at 1000 mM and the Pt_{0.5}Ni_{0.5}/g-C₃N₄ was kept at 0.100 g. Plot of the molar ratio of H₂/AB versus time for hydrogen evolution from AB catalyzed by Pt_{0.5}Ni_{0.5}/g-C₃N₄ catalyst at different temperatures are presented in Figure 8(a). As the reaction temperature from -5 °C to 10 °C, the dehydrogenation rate significantly increased. According to the slope of the straight line in Figure 8(b), the activation energy is estimated to be 38.09 kJ/mol, which is lower than most of the reported E_a values of many different Pt-based and some other catalysts [62-68].

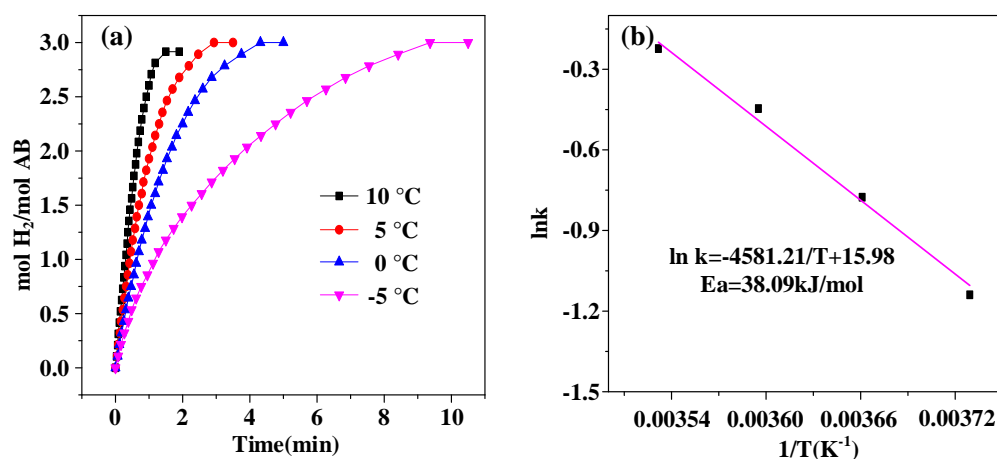
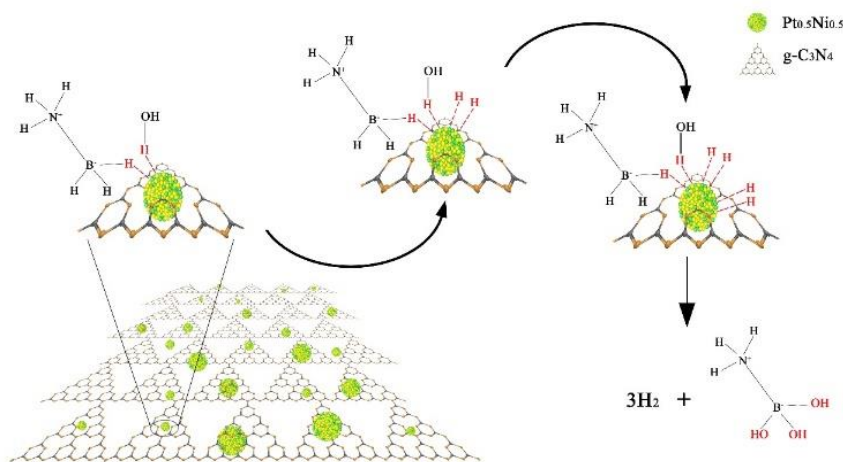


Figure 8. (a) Plot of equivalent H_2 per mole of AB versus time for hydrogen generation from AB hydrolysis catalyzed by $\text{Pt}_{0.5}\text{Ni}_{0.5}/\text{g-C}_3\text{N}_4$ catalyst at different temperatures ($[\text{Pt}_{0.5}\text{Ni}_{0.5}/\text{g-C}_3\text{N}_4] = 0.100 \text{ g}$, $[\text{AB}] = 4 \text{ mM}$), (b) Arrhenius plot of $\ln k$ vs $1/T$.



Scheme 2 Possible mechanism of hydrogen evolution from NH_3BH_3 in aqueous solution over $\text{Pt}_{0.5}\text{Ni}_{0.5}/\text{g-C}_3\text{N}_4$.

Combining the XRD, FT-IR, XPS and TEM, a possible mechanism for the hydrogen evolution from ammonia borane catalyzed by $\text{Pt}_{0.5}\text{Ni}_{0.5}/\text{g-C}_3\text{N}_4$ can be proposed. The obtained results endow persuasive and obvious evidence regarding the synergistic effects between Pt and Ni in the $\text{Pt}_{0.5}\text{Ni}_{0.5}$ NPs and the synergistic electronic effects between $\text{Pt}_{0.5}\text{Ni}_{0.5}$ nanoparticles and $\text{g-C}_3\text{N}_4$, which could efficiently activate the B–N bonds in AB, thereby lowering the reaction energy barrier and prompting hydrogen evolution, as verified by Table S1. As shown in Scheme 2, firstly, both H_2O and AB are adsorbed on the surface of the catalyst, and then, the B–H bond of AB is broken to form $\text{H}_3\text{NBH}_2\text{OH}$ by attacking BH_3^* group in H_3NBH_3 using OH^* , the OH^* further attack other B–H to dissociate hydrogen atoms. At last, the dissociated hydrogen atoms in the surface of the catalysts can combine to release hydrogen gas [69–72]. In addition, the active energy for the dehydrogenation catalyzed by $\text{Pt}_{0.5}\text{Ni}_{0.5}/\text{g-C}_3\text{N}_4$ was calculated to as low as $38.09 \text{ kJ mol}^{-1}$ and its kinetics were also obviously improved.

The stability, as a significant issue for the large-scale application of one catalyst, of the $\text{Pt}_{0.5}\text{Ni}_{0.5}/\text{g-C}_3\text{N}_4$ in the hydrolytic dehydrogenation of AB was studied and displayed in Figure 9(a). However, after 10 successive cycles, the hydrolysis of AB can also be completed within 3 min, generating a TOF value of $136.8 \text{ mol H}_2 \text{ min}^{-1} (\text{mol Pt})^{-1}$, which is only 55% of its initial catalytic activity. To further explore the reason for the decreased dehydrogenation performance, the morphology of $\text{Pt}_{0.5}\text{Ni}_{0.5}/\text{g-C}_3\text{N}_4$ after cycle test was characterized by TEM, as presented in Figure 9 (b). The slight aggregation can be observed, which may be attributed to the activity decay of $\text{Pt}_{0.5}\text{Ni}_{0.5}/\text{g-C}_3\text{N}_4$.

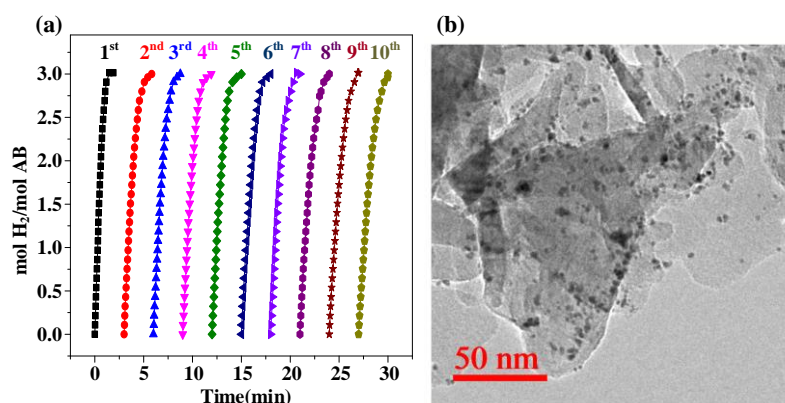


Figure 9. (a) Durability test of $\text{Pt}_{0.5}\text{Ni}_{0.5}/\text{g-C}_3\text{N}_4$ in ten runs for hydrogen generation from hydrolysis of aqueous AB solution, (b) TEM image of $\text{Pt}_{0.5}\text{Ni}_{0.5}/\text{g-C}_3\text{N}_4$ after ten cycles.

3. Materials and Methods

3.1. Materials and chemicals

Ammonia borane (NH_3BH_3 , AB, $\geq 90\%$) and melamine ($\text{C}_3\text{H}_6\text{N}_6$, $\geq 99\%$) were obtained from Aldrich. Chloroplatinic Acid (H_2PtCl_6) was supplied by Nanjing Chemical Reagent Co., Ltd. Nickel(II) chloride hexahydrate ($\text{NiCl}_2 \cdot 6\text{H}_2\text{O}$, AR), sodium hydroxide (NaOH , $\geq 96.0\%$) and sodium borohydride (NaBH_4 , $\geq 98\%$) were purchased from Sinopharm Chemical Reagent Co., Ltd. All chemicals were purchased and used without further treatment.

3.2. Synthesis of g-C₃N₄

Pure g-C₃N₄ was prepared by the direct pyrolysis of melamine, as reported by previous literatures [51,52]. Specifically, 2.00 g of melamine, placed into an alumina crucible with a cover, was annealed at 520 °C in a muffle furnace for 2 h at a ramp rate of 3 °C/min. After cooling to room temperature naturally, the resulting yellow-colored material is g-C₃N₄.

3.3. Synthesis of PtNi/g-C₃N₄

PtNi/g-C₃N₄ was fabricated *via* a simple and facile impregnation and chemical reduction method. In a typical procedure, for $\text{Pt}_{0.5}\text{Ni}_{0.5}/\text{g-C}_3\text{N}_4$, 200 mg of g-C₃N₄ and 0.4 mmol of metal precursors (0.2 mmol of H_2PtCl_6 and 0.2 mmol of NiCl_2) was firstly mixed under ultrasonic for 30 min, and then the mixture was continuously stirred for 24 hours at room temperature. After that, a mixture solution containing 0.08 g of NaBH_4 was added the above-mentioned solution at -3 °C, then stirring for 5 hours. Finally, the resulting mixture was centrifuged and dried at 80 °C in a vacuum oven. The obtained powder was denoted as $\text{Pt}_{0.5}\text{Ni}_{0.5}/\text{g-C}_3\text{N}_4$. The g-C₃N₄ supported Pt/Ni with other molar ratios could be labeled as $\text{Pt}_x\text{Ni}_{1-x}/\text{g-C}_3\text{N}_4$ ($x = 0, 0.2, 0.4, 0.6, 0.8$ and 1).

3.4. Characterization

The crystal structure of the catalysts was recorded at a scanning rate of 4 °min⁻¹ using a X-ray diffraction (XRD, Bruker D8-Advance, Cu K α radiation source ($\lambda = 0.154178$ nm)). The Fourier transformed infrared spectra (FTIR) was investigated by a Tensor 27 spectrometer (Bruker). The metal composition of the catalysts was conducted by employing inductively coupled plasma-atomic emission spectrometer (ICP-AES, Thermo iCAP6300). The specific surface area was measured using Micromeritics ASAP2020 according to adsorption/desorption nitrogen isotherms. The electronic states of the surface of the as-obtained catalyst were measured by X-ray photoelectron spectroscopy (XPS, Thermo scientific Escalab 250Xi). The morphologies and sizes of the catalysts were obtained using a Transmission electron microscope (TEM, JEOL JEM 2100F) equipped with an energy dispersive X-ray detector (EDX) at a working voltage of 200 kV. The composition of the generated gas was evaluated through a Hiden QIC-20 quadruple mass spectrometer using Ar as carrying gas.

3.5. Catalytic activity measurement

In a typical experiment, 0.1 g of the as-obtained PtNi/g-C₃N₄ was dispersed into 2 mL water in a two-necked round-bottom flask. A solution containing 2 mL of AB (2 M) was injected through one neck with a syringe under stirring, and the other was connected with a gas burette to estimate the volume of gas. Upon the injection of AB aqueous solution, the amount of H₂ production was estimated *via* water-displacement approach by measuring the volume of drained water. The reaction time was recorded as the first bubble appeared. The reaction was over when there was no gas released. The reaction was carried out under designed temperature, controlling by cryogenic bath. The reaction time was recorded as the first bubble appeared. The reaction was completed when there was no gas released. The reaction was carried out under the designed temperature, controlling by cryogenic bath. The turnover frequency (TOF, mol_{H₂} mol_{Pt}⁻¹min⁻¹) was calculated according to the linear relationship between volume and time in AB hydrolysis.

In order to explore the influence of catalysts concentration, AB concentration over the dehydrogenation of AB, AB hydrolysis for the Pt_{0.5}Ni_{0.5}/g-C₃N₄ was evaluated in the same way as described above, except that the parameters, such as catalysts concentration, AB concentration, were changed, respectively. In addition, to acquire the activation energy (*E_a*) value of the hydrogen production of AB over Pt_{0.5}Ni_{0.5}/g-C₃N₄ catalyst, the hydrolysis of AB was conducted at a series of temperatures including -5 °C, 0 °C, 5 °C and 10 °C.

3.6. Stability tests

The catalyst was recovered and washed with ethanol and water after the completion of dehydrogenation reaction. And then the recovered catalyst was set into a two-necked round-bottom flask according to the above-mentioned dehydrogenation procedure for stability tests. A similar operation was repeated ten times.

4. Conclusions

In summary, we report a simple and facile impregnation and chemical reduction approach to synthesize PtNi/g-C₃N₄ nanoparticles as catalyst for boosting the hydrogen generation of AB. Among the Pt_xNi_{1-x}/g-C₃N₄ catalysts, the resultant Pt_{0.5}Ni_{0.5}/g-C₃N₄ catalyst demonstrates outstanding performance, including 100% conversion, 100% H₂ selectivity, yielding the extraordinary initial total turnover frequency (TOF) of 250.8 mol_{H₂} min⁻¹ (mol_{Pt})⁻¹ for hydrogen production from AB at 10 °C, a relatively low activation energy of 38.09 kJ mol⁻¹, and a remarkable reusability (at least 10 times), which outperform most of the noble metal heterogeneous catalysts. This notably improved activity is attributed to the charge interaction between PtNi NPs and g-C₃N₄ support. Especially, the nitrogen-containing functional groups on g-C₃N₄, serving as the anchoring sites for PtNi NPs, may be beneficial for forming a uniform distribution and decreasing the particle size for the NPs. Moreover, the fabrication of g-C₃N₄-based catalysts may prompt the utilization of g-C₃N₄ in energy fields.

Supplementary Materials: The following are available online at www.mdpi.com/xxx/s1, Figure S1: XPS spectra for Pt_{0.5}Ni_{0.5}/g-C₃N₄ showing C 1s, N 1s, Figure S2: (a) TEM images of Ni/g-C₃N₄, (b) amplified HRTEM image of Ni/g-C₃N₄, (c) Particle size distribution of Ni/g-C₃N₄, (d) TEM images of Pt/g-C₃N₄, (e) amplified HRTEM image of Pt/g-C₃N₄, (f) Particle size distribution of Pt/g-C₃N₄, Figure S3: SEM-energy-dispersive X-ray spectroscopic (EDS) spectrum of Pt_{0.5}Ni_{0.5}/g-C₃N₄, Table S1: ICP-AES results of PtNi/g-C₃N₄ catalysts.

Author Contributions: Data curation, M.Z.; Writing—original draft, X.X.; Investigation, Y.W.; Formal analysis, Y.A.; Funding acquisition, L.X.; Supervision, Writing – review & editing, C.W.

Funding: This work was financially supported by Anhui Provincial Natural Science Foundation (1608085QF156, 1908085QB68), the Natural Science Foundation of the Anhui Higher Education Institutions of China (KJ2019A0072), Foundation of Zhejiang Provincial Key Laboratory of Advanced Chemical Engineering Manufacture Technology (Grant No. ZJKL-ACEMT-1802), Research Fund for Young Teachers of Anhui University of Technology (QZ201610) and National Natural Science Foundation of China (21376005).

Conflicts of Interest: The authors declare no conflict of interest.

References

1. Graetz, J. New approaches to hydrogen storage. *Chem. Soc. Rev.* **2009**, *38*, 73–82.
2. Yu, X.B.; Tang, Z.W.; Sun, D.L.; Ouyang, L.Z.; Zhu, M. Recent advances and remaining challenges of nanostructured materials for hydrogen storage applications. *Prog. Mater. Sci.* **2017**, *88*, 1–48.
3. He, T.; Pachfule, P.; Wu, H.; Xu, Q.; Chen, P. Hydrogen carriers. *Nat. Rev. Mater.* **2016**, *1*, 16059.
4. Liu, T.; Wang, Q.T.; Yuan, J.Z.; Zhao, X.; Gao, G.H. Highly Dispersed Bimetallic Nanoparticles Supported on Titanium Carbides for Remarkable Hydrogen Release from Hydrous Hydrazine. *ChemCatChem* **2018**, *10*, 2200–2204.
5. Yadav, M.; Xu, Q. Liquid-phase chemical hydrogen storage materials. *Energy Environ. Sci.* **2012**, *5*, 9698–9725.
6. Schlapbach, L.; Züttel, A. Hydrogen-storage materials for mobile applications. *Materials for Sustainable Energy* **2010**, 265–270.
7. Yao, F.; Li, X.; Wan, C.; Xu, L.X.; An, Y.; Ye, M.F.; Lei, Z. Highly efficient hydrogen release from formic acid using a graphitic carbon nitride-supported AgPd nanoparticle catalyst. *Appl. Surf. Sci.* **2017**, *426*, 605–611.
8. Staubitz, A.; Robertson, A.P.M.; Manners, I. Ammonia-Borane and related compounds as dihydrogen sources. *Chem. Rev.* **2010**, *110*, 4079–4124.
9. Zhou, Y.-H.; Wang, S.Q.; Zhang, Z.Y.; Williams, N.; Cheng, Y.; Gu, J. Hollow Nickel–Cobalt Layered Double Hydroxide Supported Palladium Catalysts with Superior Hydrogen Evolution Activity for Hydrolysis of Ammonia Borane. *ChemCatChem* **2018**, *10*, 3206–3213.
10. Huang, X.Y.; Wang, A.J.; Zhang, L.; Fang, K.M.; Wu, L.J.; Feng, J.J. Melamine-assisted solvothermal synthesis of PtNi nanodendrites as highly efficient and durable electrocatalyst for hydrogen evolution reaction. *J. Colloid. Interf. Sci.* **2018**, *531*, 578–584.
11. Wan, C.; Yao, F.; Li, X.; Hu, K.; Ye, M.F.; Xu, L.X.; An, Y. Bimetallic AgPd Nanoparticles Immobilized on Amine-Functionalized SBA-15 as Efficient Catalysts for Hydrogen Generation from Formic Acid. *ChemistrySelect* **2016**, *1*, 6907–6913.
12. Chen, J.M.; Lu, Z.H.; Yao, Q.L.; Feng, G.; Luo, Y. Complete dehydrogenation of $N_2H_4BH_3$ with Ni-MCr₂O₃ (M=Pt, Rh, and Ir) hybrid nanoparticles. *J. Mater. Chem. A* **2018**, *6*, 20746–20752.
13. Zhang, L.T.; Cai, Z.L.; Yao, Z.D.; Ji, L.; Sun, Z.; Yan, N.H.; Zhang, B.Y.; Xiao, B.B.; Du, J.; Zhu, X.Q.; Chen, L.X.; A striking catalytic effect of facile synthesized ZrMn₂ nanoparticles on the de/rehydrogenation properties of MgH₂. *J. Mater. Chem. A* **2019**, *7*, 5626–5634.
14. Akbayrak, S.; Özçifçi, Z.; Tabak, A. Regular Article Noble metal nanoparticles supported on activated carbon: Highly recyclable catalysts in hydrogen generation from the hydrolysis of ammonia borane. *J. Colloid Interf. Sci.* **2019**, *546*, 324–332.
15. Qu, X.P.; Jiang, R.; Li, Q.; Zeng, F.N.; Zheng, X.; Xu, Z.M.; Chen, C.H.; Peng, J. The hydrolysis of ammonia borane catalyzed by NiCoP/OPC-300 nanocatalysts: high selectivity and efficiency, and mechanism. *Green Chem.* **2019**, *21*, 850–860.
16. Li, J.; Li, F.; Liao, J.; Liu, Q.; Li, H. Cu_{0.4}Co_{0.6}MoO₄ Nanorods Supported on Graphitic Carbon Nitride as a Highly Active Catalyst for the Hydrolytic Dehydrogenation of Ammonia Borane. *Catalysts* **2019**, *9*, 714.
17. Torres, D.A.; Garcia, M.N.; Mori, K.; Kuwahara, Y.; Yamashita, H. Nitrogen-doped carbon materials as a promising platform toward the efficient catalysis for hydrogen generation, *Appl. Catal. A, General* **2019**, *571*, 25–41.
18. Bandaru, S.; English, N.J.; Phillips, A.D.; MacElroy, J.M.D. Exploring Promising Catalysts for Chemical Hydrogen Storage in Ammonia Borane: A Density Functional Theory Study. *Catalysts* **2017**, *7*, 140.
19. Wei, Z.H.; Liu, Y.; Peng, Z.K.; Song, H.Q.; Liu, Z.Y.; Liu, B.Z.; Li, B.J.; Yang, B.; Lu, S.Y. Cobalt-Ruthenium Nanoalloys Parceled in Porous Nitrogen-Doped Graphene as Highly Efficient Difunctional Catalysts for Hydrogen Evolution Reaction and Hydrolysis of Ammonia Borane. *ACS Sustainable Chem. Eng.* **2019**, *7*, 7014–7023.
20. Chen, W.Y.; Wang, Z.J.; Duan, X.Z.; Qian, G.; Chen, D.; Zhou, X.G. Structural and kinetic insights into Pt/CNT catalysts during hydrogen generation from ammonia borane. *Chem. Eng. Sci.* **2018**, *192*, 1242–1251.
21. Xu, C.L.; Wang, H.; Wang, Q.; Wang, Y.; Zhang, Y.; Fan, G.Y. Ruthenium coordinated with triphenylphosphine-hyper-crosslinked polymer: An efficient catalyst for hydrogen evolution reaction and hydrolysis of ammonia borane. *Appl. Surf. Sci.* **2019**, *466*, 193–201.

22. Zhang, J.K.; Chen, W.Y.; Ge, H.B.; Chen, C.Q.; Yan, W.J.; Gao, Z.; Gan, J.; Zhang, B.Y.; Duan, X.Z.; Qin, Y. Synergistic effects in atomic-layer-deposited PtCo_x/CNTs catalysts enhancing hydrolytic dehydrogenation of ammonia borane. *Appl. Catal. B* **2018**, *235*, 256–263.
23. Liu, Y.; Zhang, J.; Guan, H.J.; Zhao, Y.F.; Yang, J.H.; Zhang, B. Preparation of bimetallic Cu-Co nanocatalysts on poly (diallyldimethylammonium chloride) functionalized halloysite nanotubes for hydrolytic dehydrogenation of ammonia borane. *Appl. Surf. Sci.* **2018**, *427*, 106–113.
24. Hou, C.C.; Li, Q.; Wang, C.J.; Peng, C.Y.; Chen, Q.Q.; Ye, H.F.; Fu, W.F.; Che, C.M.; López, N.; Chen, Y. Ternary Ni–Co–P nanoparticles as noble-metal-free catalysts to boost the hydrolytic dehydrogenation of ammonia-borane. *Energy Environ. Sci.* **2017**, *10*, 1770–1776.
25. Zhao, W.; Wang, R.Y.; Wang, Y.; Feng, J.W.; Li, C.C.; Chen, G.Z. Effect of LDH composition on the catalytic activity of Ru/LDH for the hydrolytic dehydrogenation of ammonia borane. *Int. J. Hydrogen Energy* **2019**, *44*, 14820–14830.
26. Özhava, D.; Özkar, S. Nanoceria supported rhodium(0) nanoparticles as catalyst for hydrogen generation from methanolysis of ammonia borane. *Appl. Catal. B* **2018**, *237*, 1012–1020.
27. Akbayrak, S.; Özkar, S. Ammonia borane as hydrogen storage materials. *Int. J. Hydrogen Energy* **2018**, *43*, 18592–18606.
28. Wen, M.; Wu, Q.N.; Peng, J.; Wu, Q.S.; Wang, C.X. Fabrication of Pt-loaded NiCo nanochains with superior catalytic dehydrogenation activity. *J. Colloid Interf. Sci.* **2014**, *416*, 220–226.
29. Wan, C.; Cheng, D.G.; Chen, F.Q.; Zhan, X.L. Fabrication of CeO₂ nanotube supported Pt catalyst encapsulated with silica for high and stable performance. *Chem. Commun.* **2015**, *51*, 9785–9788.
30. Wang, S.; Zhang, D.; Ma, Y.Y.; Zhang, H.; Gao, J.; Nie, Y.T.; Sun, X.H. Aqueous solution synthesis of Pt-M (M=Fe, Co, Ni) bimetallic nanoparticles and their catalysis for the hydrolytic dehydrogenation of ammonia borane. *ACS Appl. Mater. Interfaces* **2014**, *6*, 12429–12435.
31. Du, Y.S.; Su, J.; Luo, W.; Cheng, G.Z. Graphene-Supported Nickel-Platinum Nanoparticles as Efficient Catalyst for Hydrogen Generation from Hydrous Hydrazine at Room Temperature. *ACS Appl. Mater. Interfaces* **2015**, *7*, 1031–1034.
32. Zhao, B.H.; Feng, K.; Wang, Y.; Lv, X.X.; Zheng, H.C.; Ma, Y.Y.; Yan, W.S.; Sun, X.H.; Zhong, J. Pt_xNi_{10-x}O nanoparticles supported on N-doped graphene oxide with a synergetic effect for highly efficient hydrolysis of ammonia borane. *Catal. Sci. Technol.* **2017**, *7*, 5135–5142.
33. Y. Xia, J.R. Ye, D.G. Cheng, F.Q. Chen, X.L. Zhan, Identification of a flattened Pd–Ce oxide cluster as a highly efficient catalyst for low-temperature CO oxidation. *Catal. Sci. Technol.* **2018**, *8*, 5137–5147.
34. Huang, X.Y.; Zhu, X.Y.; Zhang, X.F.; Zhang, L.; Feng, J.J.; Wang, A.J. Simple solvothermal synthesis of uniform Pt₆₆Ni₃₄ nanoflowers as advanced electrocatalyst to significantly boost the catalytic activity and durability of hydrogen evolution reaction. *Electrochim. Acta* **2018**, *271*, 397–405.
35. Chen, X.L.; Zhang, H.X.; Huang, X.Y.; Feng, J.J.; Han, D.M.; Zhang, L.; Chen, J.R.; Wang, A.J. Facile solvothermal fabrication of Pt₄₇Ni₅₃ nanopolyhedrons for greatly boosting electrocatalytic performances for oxygen reduction and hydrogen evolution. *J. Colloid. Interf. Sci.* **2018**, *525*, 260–268.
36. Karaca, T.; Sevim, M.; Metin, Ö. Facile Synthesis of Monodisperse Copper–Platinum Alloy Nanoparticles and Their Superb Catalysis in the Hydrolytic Dehydrogenation of Ammonia Borane and Hydrazine Borane. *ChemCatChem* **2017**, *9*, 4185–4190.
37. Zhang, H.M.; Ke, D.D.; Cheng, L.N.; Feng, X.L.; Hou, X.W.; Wang, J.; Lia, Y.; Han, S.M. CoPt-Co hybrid supported on amino modified SiO₂ nanospheres as a high performance catalyst for hydrogen generation from ammonia borane. *Sci.-Mater.* **2019**, *29*, 1–9.
38. Zhou, Q.X.; Qi, L.; Yang, H.X.; Xu, C.X. Hierarchical nanoporous platinum–copper alloy nanoflowers as highly active catalysts for the hydrolytic dehydrogenation of ammonia borane. *J. Colloid. Interf. Sci.* **2018**, *513*, 258–265.
39. Ge, Y.Z.; Ye, W.Y.; Shah, Z.H. Lin, X.J.; Lu, R.W.; Zhang, S.F. PtNi/NiO Clusters Coated by Hollow Silica: Novel Design for Highly Efficient Hydrogen Production from Ammonia–Borane. *ACS Appl. Mater. Interfaces* **2017**, *9*, 3749–3756.
40. Zhou, Q.X.; Xu, C.X. Nanoporous PtCo/Co₃O₄ composites with high catalytic activities toward hydrolytic dehydrogenation of ammonia borane. *J. Colloid. Interf. Sci.* **2017**, *508*, 542–550.
41. Chen, W.Y.; Ji, J.; Feng, X.; Duan, X.Z.; Qian, G.; Li, P.; Zhou, X.G.; Chen, D.; Yuan, W.K. Mechanistic Insight into Size-Dependent Activity and Durability in Pt/CNT Catalyzed Hydrolytic Dehydrogenation of Ammonia Borane. *J. Am. Chem. Soc.* **2014**, *136*, 16736–16739.

42. Kamegawa, T.; Nakaue, T. Complete hydrogen release from aqueous ammonia-borane over a platinum-loaded titanium dioxide photocatalyst. *Chem. Commun.* **2015**, *51*, 16802–16805.
43. Zhu, M.Y.; Xu, L.X.; Du, L.; An, Y.; Wan, C. Palladium supported on carbon nanotubes as a high-performance catalyst for the dehydrogenation of dodecahydro-N-ethylcarbazole. *Catalysts* **2018**, *8*, 638.
44. Ke, D.D.; Wang, J.; Zhang, H.M.; Li, Y.; Zhang, L.; Zhao, X.; Han, S.M. Fabrication of Pt-Co NPs supported on nanoporous graphene as high-efficient catalyst for hydrolytic dehydrogenation of ammonia borane. *Int. J. Hydrogen Energy* **2017**, *42*, 26617–26625.
45. Wang, C.L.; Tuninetti, J.; Wang, Z.; Zhang, C.; Ciganda, R.; Salmon, L.; Moya, S.; Ruiz, J.; Astruc, D. Hydrolysis of Ammonia-Borane over Ni/ZIF-8 Nanocatalyst: High Efficiency, Mechanism, and Controlled Hydrogen Release. *J. Am. Chem. Soc.* **2017**, *139*, 11610–11615.
46. Wang, W.; Lu, Z.H.; Luo, Y.; Zou, A.H.; Yao, Q.L.; Chen, X.S. Mesoporous Carbon Nitride Supported Pd and Pd-Ni Nanoparticles as Highly Efficient Catalyst for Catalytic Hydrolysis of NH_3BH_3 . *ChemCatChem* **2018**, *10*, 1620–1626.
47. Han, C.H.; Meng, P.; Waclawik, E.R.; Zhang, C.; Li, X.H.; Yang, H.Q.; Antonietti, M.; Xu, J.S. Palladium/Graphitic Carbon Nitride (g- C_3N_4) Stabilized Emulsion Microreactor as a Store for Hydrogen from Ammonia Borane for Use in Alkene Hydrogenation. *Angew. Chem. Int. Ed.* **2018**, *57*, 14857–14861.
48. Ong, W.J.; Tan, L.L.; Ng, Y.H.; Yong, S.T.; Chai, S.P. Graphitic Carbon Nitride (g- C_3N_4)-Based Photocatalysts for Artificial Photosynthesis and Environmental Remediation: Are We a Step Closer To Achieving Sustainability? *Chem. Rev.* **2016**, *116*, 7159–7329.
49. Guo, L.T.; Cai, Y.Y.; Ge, J.M.; Zhang, Y.N.; Gong, L.H.; Li, X.H.; Wang, K.X.; Ren, Q.Z.; Su, J.; Chen, J.S. Multifunctional Au-Co@CN Nanocatalyst for Highly Efficient Hydrolysis of Ammonia Borane. *ACS Catal.* **2015**, *5*, 388–392.
50. Lu, R.; Hu, M.; Xu, C.L.; Wang, Y.; Zhang, Y.; Xu, B.; Gao, D.J.; Bi, J.; Fan, G.Y. Hydrogen evolution from hydrolysis of ammonia borane catalyzed by Rh/g- C_3N_4 under mild conditions. *Int. J. Hydrogen Energy* **2018**, *43*, 7038–7045.
51. Wang, X.C.; Blechert, S.; Antonietti, M. Polymeric Graphitic Carbon Nitride for Heterogeneous Photocatalysis. *ACS Catal.* **2012**, *2*, 1596–1606.
52. Xu, L.X.; Liu, N.; Hong, B.; Cui, P.; Cheng, D.G.; Chen, F.Q.; An, Y.; Wan, C. Nickel-platinum nanoparticles immobilized on graphitic carbon nitride as highly efficient catalyst for hydrogen release from hydrous hydrazine. *RSC Adv.* **2016**, *6*, 31687–31691.
53. Fu, F.Y.; Wang, C.L.; Wang, Q.; Martinez-Villacorta, A.M. Highly Selective and Sharp Volcano-type Synergistic Ni₂Pt@ZIF-8-Catalyzed Hydrogen Evolution from Ammonia Borane Hydrolysis. *J. Am. Chem. Soc.* **2018**, *140*, 10034–10042.
54. Jiao, W.L.; Hu, X.P.; Ren, H.; Xu, P.F.; Yu, R.B.; Chen, J.; Xing, X.R. Magnetic Ni and Ni/Pt hollow nanospheres and their catalytic activities for hydrolysis of ammonia borane. *J. Mater. Chem. A* **2014**, *2*, 18171–18176.
55. Li, Z.; He, T.; Matsumura, D.J.; Miao, S.; Wu, A.A.; Liu, L.; Wu, G.T.; Chen, P. Atomically Dispersed Pt on the Surface of Ni Particles: Synthesis and Catalytic Function in Hydrogen Generation from Aqueous Ammonia-Borane. *ACS Catal.* **2017**, *7*, 6762–6769.
56. Cao, N.; Su, J.; Luo, W.; Cheng, G.Z. Ni-Pt nanoparticles supported on MIL-101 as highly efficient catalysts for hydrogen generation from aqueous alkaline solution of hydrazine for chemical hydrogen storage. *Int. J. Hydrogen Energy* **2014**, *39*, 9726–9734.
57. Yao, Q.L.; Lu, Z.H.; Huang, W.; Chen, X.S.; Zhu, J. High Pt-like activity of the Ni-Mo/graphene catalyst for hydrogen evolution from hydrolysis of ammonia borane. *J. Mater. Chem. A* **2016**, *4*, 8579–8583.
58. Wan, C.; Sun, L.; Xu, L.X.; Cheng, D.G.; Chen, F.Q.; Zhan, X.L.; Yang, Y.R. Novel NiPt alloy nanoparticle decorated 2D layered g- C_3N_4 nanosheets: a highly efficient catalyst for hydrogen generation from hydrous hydrazine. *J. Mater. Chem. A* **2019**, *7*, 8798–8804.
59. Aranishi, K.; Singh, A.K.; Xu, Q. Dendrimer-encapsulated bimetallic Pt-Ni nanoparticles as highly efficient catalysts for hydrogen generation from chemical hydrogen storage materials. *ChemCatChem* **2013**, *5*, 2248–2252.
60. Yang, X.J.; Cheng, F.Y.; Liang, J.; Tao, Z.L.; Chen, J. Carbon-supported Ni_{1-x}@Pt_x (x=0.32, 0.43, 0.60, 0.67, and 0.80) core-shell nanoparticles as catalysts for hydrogen generation from hydrolysis of ammonia borane. *Int. J. Hydrogen Energy* **2011**, *36*, 1984–1990.

61. Zhang, M.Y.; Liu, L.; Lu, S.; Xu, L.X.; An, Y.; Wan, C. Facile Fabrication of NiPt/CNTs as an Efficient Catalyst for Hydrogen Production from Hydrous Hydrazine. *ChemistrySelect* **2019**, *4*, 10494–10500.
62. Hu, Y.J.; Wang, Y.Q.; Lu, Z.H.; Chen, X.S.; Xiong, L.H. Core-shell nanospheres Pt@SiO₂ for catalytic hydrogen production. *Appl. Surf. Sci.* **2015**, *341*, 185–189.
63. Zhou, Q.X.; Xu, C.X. Nanoporous PtRu alloys with unique catalytic activity toward hydrolytic dehydrogenation of ammonia borane. *Chem. Asian J.* **2016**, *11*, 705–712.
64. Cao, N.; Hu, K.; Luo, W.; Cheng, G.Z. RuCu nanoparticles supported on graphene: a highly efficient catalyst for hydrolysis of ammonia borane. *J. Alloys Compd.* **2014**, *590*, 241–246.
65. Wang, X.; Liu, D.P.; Song, S.Y.; Zhang, H.J. Graphene oxide induced formation of Pt–CeO₂ hybrid nanoflowers with tunable CeO₂ thickness for catalytic hydrolysis of ammonia borane. *Chem.–Eur. J.* **2013**, *19*, 8082–8086.
66. Rachiero, G.P.; Demirci, U.B.; Miele, P. Bimetallic RuCo and RuCu catalysts supported on γ -Al₂O₃ a comparative study of their activity in hydrolysis of ammonia-borane. *Int. J. Hydrogen Energy* **2011**, *36*, 7051–7065.
67. Yang, X.J.; Cheng, F.Y.; Liang, J.; Tao, Z.L.; Chen, J. Pt₁Ni_{1-x} nanoparticles as catalysts for hydrogen generation from hydrolysis of ammonia borane. *Int. J. Hydrogen Energy* **2009**, *34*, 8785–8791.
68. Rakap, M. Poly(N-vinyl-2-pyrrolidone)-stabilized palladium-platinum nanoparticles-catalyzed hydrolysis of ammonia borane for hydrogen generation, *J. Power Sources* **2015**, *276*, 320–327.
69. Kalidendi, S.B.; Sanyal, U.; Jagirdar, B.R. Nanostructured Cu and Cu@Cu₂O core shell catalysts for hydrogen generation from ammonia-borane. *Phys. Chem. Chem. Phys.* **2008**, *10*, 5870–5874.
70. Ma, H.; Na, C. Isokinetic Temperature and Size-Controlled Activation of Ruthenium-Catalyzed Ammonia Borane Hydrolysis. *ACS Catal.* **2015**, *5*, 1726–1735.
71. Gao, M.Y.; Yang, W.W.; Yu, Y.S. Monodisperse PtCu alloy nanoparticles as highly efficient catalysts for the hydrolytic dehydrogenation of ammonia borane. *Int. J. Hydrogen Energy* **2018**, *43*, 14293–14300.
72. Xu, D.; Wang, W.D.; Tian, M.; Dong, Z.P. Immobilization of Pt nanoparticles in hollow mesoporous silica nanocapsules: An aggregation- and leaching-resistant catalyst. *J. Colloid Interf. Sci.* **2018**, *516*, 407–415.